

Kinematic and Prototype Research of A Novel Three-wire-driven Parallel (TWDP) Robot

Tao Yu*, School of Electromechanical Automobile Engineering, Yantai University, China, yt_126@126.com

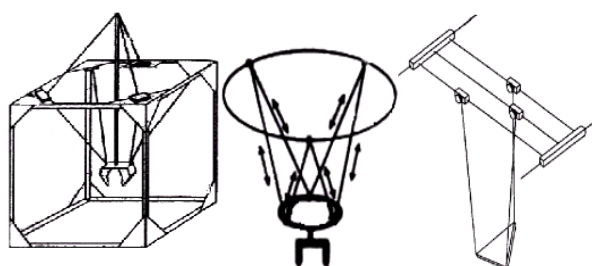
Qingkai Han, School of Mechanical Engineering and Automation, Northeastern University, China, qhan@mail.neu.edu.cn

Abstract: In the paper, a novel new gravity-constrained (GC) three-wire-driven (TWD) parallel robot is proposed, and the prototype is presented with control system. With its mechanism model, three typical kinematic analytical models, including horizontal up-down motion, pitching motion and heeling motion and their corresponding simulations are given in detail. The open-loop and close-loop control scheme are used separately to realize the motion control of the robot. Especially, the image processing based machine vision is adopted firstly in the close-loop control of wire-driven robot. At last, the error analysis of the robot is given in detail.

Key-Words: Wire-driven, Parallel robot, Kinematics, Statics, Motion control, Machine vision

1. Introduction

The wire-driven mechanism, a kind of mechanism using wire or tendon to transform power and motion, has advantages of lighter mass, lower price and more widely workspace than that driven by hydraulic cylinder or lead screw. So more and more wire-driven mechanism or robot are designed and studied[1-3].



(a) FALCON-7 (b) NIST ROBOCRANE (c) CABLEV

Fig. 1 Several kinds of wire-driven-parallel robot

In 1995, a new high speed parallel robot named “FALCON-7”[4] driven by tensioned wire with rigidity was

firstly reported by S. Kawamura on the international conference of robot and automation, which attracted widely attention of international scholar. After that, some new kinds of wire-driven parallel robots are proposed, such as “NIST ROBOCRANE” by J. Albus[5] and “CABLEV”[6] by Thomas Maier, etc., as shown in Fig.1.

If taking the driving wire’s number as m and degree of freedom of manipulator as n , this kind of robot can be categorized as Incompletely Restrained Positioning Mechanism (IRPM, $m \leq n$), Completely Restrained Positioning Mechanism (CRPM, $m = n + 1$), and Redundantly Restrained Positioning Mechanism (RRPM, $m > n + 1$). In the paper, a novel gravity-constrained 3 wire-driven IRPM parallel robot is designed. Compared with previous wire-driven mechanism (as shown in Fig.1), the robot proposed here has simplest structure which can realize specific motion.

By the robot mechanism model, three typical kinematic analytical models, including horizontal up-down motion, pitching motion and heeling motion, and their corresponding simulations are given in detail. Also, the corresponding

prototype is manufactured to carry out experiments of motion control and position localizing. In the motion control experiment, the open-loop and close-loop control strategy are used separately. Especially in close-loop control experiment, the machine vision based techniques is adopted to control the position of manipulator of robot.

2. Construction of the Robot and Degree of Freedom Analysis

2.1 Construction of the Robot

The robot consists of base, platform(manipulator), pulley, pillar, wire and motor, as shown in Fig. 2. Through adjusting of the length of the wire, the position and attitude of the platform can be controlled.

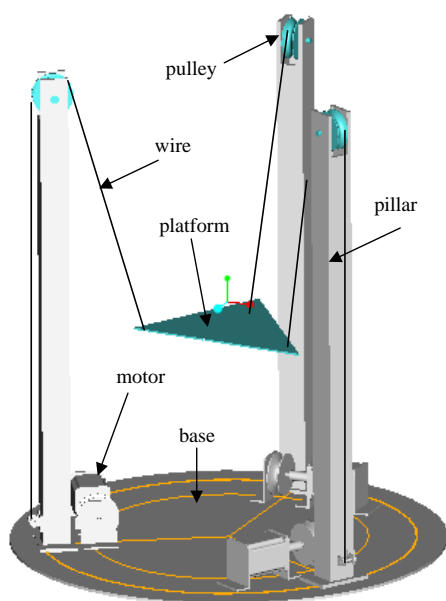


Fig. 2 Structure of robot

The platform's shape is isosceles triangular. Each corner of the platform is connected with one end of a strip of wire, and the other end is wrapped around the shaft of the motor through the big pulley on the top the pillar and the small pulley at the bottom of the pillar consequently. By the gravity of platform itself, the wires are tensioned. Thus, a novel gravity-constrained (GC) three-wire-driven (TWD) parallel robot is proposed.

2.2 Construction of the Robot

From Fig. 2, the mechanism of the robot can be obtained as shown in Fig.3, in which O is global coordinate and o is local coordinate of platform. Each strip of the wire can be viewed as an combination of a shifting pare and a revolute pare. At three top ends of the pillars and the three corners of the platform, the wires can be regarded as six Hooke pares. When the length of the wire, that is, l_1 and l_2 respectively, is determined, the position and attitude of platform can be determined. From the analysis of the Fig.3, the platform can move translational along the Z axis, called up-down motion, and rotate around X and Y axis, called heeling and pitching motion respectively. Thus, the robot can be treated as a three freedom system.

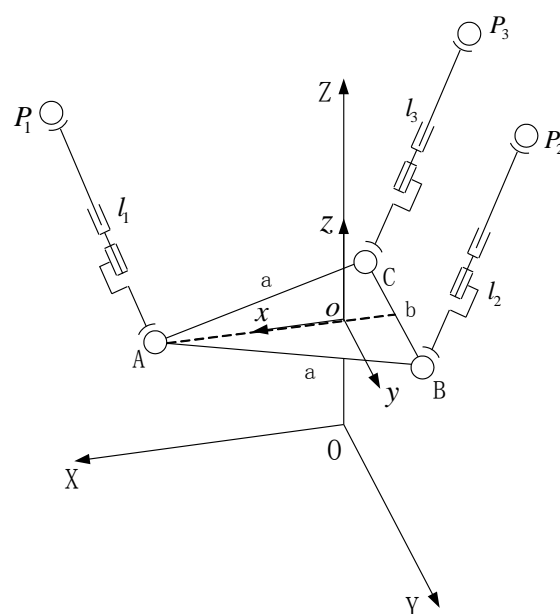


Fig. 3 Machanism of the robot

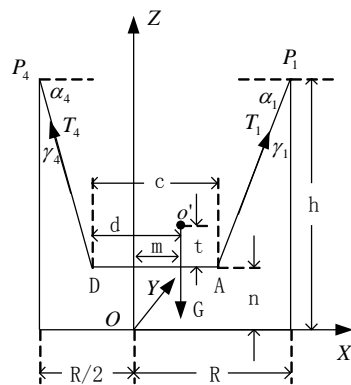
3. Kinematic Analysis and Simulation

Three typical motions, e.g. horizontal up-down motion, pitching motion and heeling motion are discussed in this part.

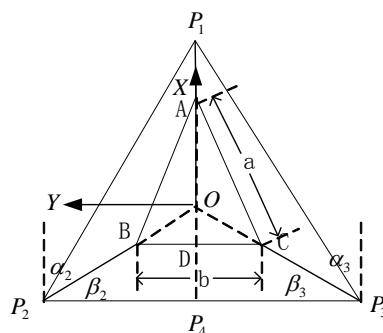
3.1 Horizontal up-down motion

In this motion, the platform moves symmetrically with X axis. The spatial problem can be transferred as a planar problem, as shown in Fig.4 (a) and Fig.4 (b).

The structural parameters of the robot are, $t=0$ mm, $R=247.5$ mm, $b=250$ mm, $d=91$ mm, $c=273$ mm, $h=750$ mm, and $G=2$ N, where t is the vertical distance from the center of gravity of loaded platform to the base. R is the radius of circle where the pillars locate. b is the length of base of isosceles triangle platform. d is the distance from o' to platform. c is the distance from the top of platform to the base edge. h is the height of pillar. G is the total gravity of platform and loads. The tensions in the wire P_1A , P_2B and P_3C are identified as T_1 , T_2 , and T_3 . A piece of virtual wire P_4D is introduced for the convenience of analysis, the endpoint P_4 and D are located as the middle of P_2P_3 and BC . In general case, the platform together with loads are considered as a whole body, which is called manipulating target. The centre-of-gravity position is o' , as shown in Fig.4(a).



(a) side view



(b) top view

Fig. 4 The horizontal up-down situation of platform

By using force balancing, torque balancing and

geometrical relationship of robot structure, the following equations can be established in the global coordinates.

$$\begin{cases} l_1 \cos \alpha_1 + c + l_4 \cos \alpha_4 = 3R / 2 \\ l_1 \cos \gamma_1 = l_4 \cos \gamma_4 \\ T_1 \cos \gamma_1 + T_4 \cos \gamma_4 = G \\ T_1 \cos \alpha_1 = T_4 \cos \alpha_4 \\ T_4 \cos \alpha_4 \cdot n - T_4 \cos \gamma_4 (d - m) + T_1 \cos \gamma_1 \\ (m + c - d) - T_1 \cos \alpha_1 \cdot n - G \cdot m = 0 \\ l_1 \cos \gamma_1 + n = h \end{cases} \quad (1)$$

Where, $\alpha_i, \beta_i, \gamma_i, (i=1, \dots, 4)$ are the angles between the i th wire and the X, Y and Z axis. The relation of $\cos \gamma_1 = \sin \alpha_1$ can be obtained by the trigonometry. l_1, l_2, l_3 and l_4 are the length of wire P_1A, P_2B and P_3C respectively. n is the distance from the platform to base of robot, and vary from 100 mm to 500 mm.

The equation set (1) can be simplified as

$$\begin{cases} l_1 \cos \alpha_1 + c + l_4 \cos \alpha_4 = 3R / 2 \\ l_1 \sin \alpha_1 = l_4 \sin \alpha_4 \\ T_1 \sin \alpha_1 + T_4 \sin \alpha_4 = G \\ T_1 \cos \alpha_1 = T_4 \cos \alpha_4 \\ T_1 \sin \alpha_1 \cdot c = G \cdot d \\ l_1 \sin \alpha_1 + n = h \end{cases} \quad (2)$$

Exam the equation set (2), for every specific height n , the only status of the wires is corresponded with only solution of $\alpha_1, \alpha_4, T_1, T_4, l_1$, and l_4 . That is,

$$\begin{cases} \alpha_1 = \arctan \frac{h-n}{\frac{c-d}{c}(\frac{3R}{2}-c)} \\ \alpha_4 = \arctan \frac{h-n}{\frac{d}{c}(\frac{3R}{2}-c)} \\ l_1 = \frac{h-n}{\sin \alpha_1}, l_4 = \frac{h-n}{\sin \alpha_4} \\ T_1 = \frac{G \cdot d}{\sin \alpha_1 \cdot c}, T_4 = \frac{G \cdot (c-d)}{\sin \alpha_4 \cdot c} \end{cases} \quad (3)$$

Also, the length of wire P_2B and P_3C can be obtained through P_4D , that is

$$l_2 = l_3 = \sqrt{l_4^2 + \frac{(\sqrt{3}R - b)^2}{4}} \quad (4)$$

The simulation results are shown in Fig. 5.

The Fig.6 show us the linear relation between the changes of platform's height n and wire's length $l_1(l_2)$ when horizontal up-down motion, which can improve the stability of robot movement.

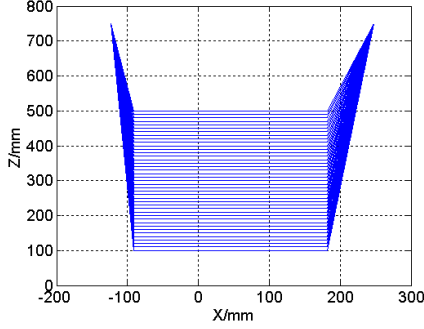


Fig. 5 The simulation of platform's horizontal up-down motion(side view)

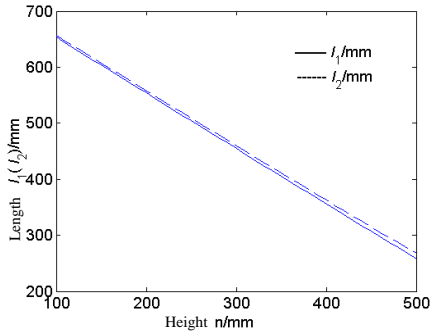


Fig. 6 The relation between the changes of platform's height n and wire's length $l_1(l_2)$ when horizontal up-down motion

3.2 Pitching motion

From Fig. 7, the kinematic equations of pitching motion can be written as

$$\begin{cases} l_1 \cos \alpha_1 + c \cos \theta + l_4 \cos \alpha_4 = 3R/2 \\ l_1 \sin \alpha_1 = c \sin \theta + l_4 \sin \alpha_4 \\ l_1 \sin \alpha_1 + n - (c-d) \sin \theta - t \cos \theta = h \\ T_1 \sin \alpha_1 + T_4 \sin \alpha_4 = G \\ T_1 \cos \alpha_1 = T_4 \cos \alpha_4 \\ T_1 \sin \alpha_1 \cdot c \cdot \cos \theta + T_1 \cos \alpha_1 \cdot c \cdot \sin \theta \\ = G(d \cdot \cos \theta + t \sin \theta) \end{cases} \quad (5)$$

The equation set (5) has 6 equations and 7 unknown

variables $\alpha_1, \alpha_4, T_1, T_4, l_1, l_4$ and θ . For every specific n and θ , the equation set (5) has unique solutions. To simplify the solving process, the special solving method is adopted here. By assuming several unknown variables as known and according the structure of robot and geometrical relationship, the other unknown variables can be expressed by the known. Then the solutions are judged by the given criteria.

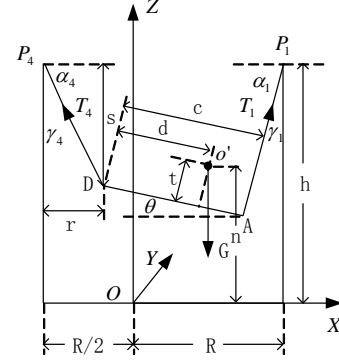


Fig. 7 Platform's pitching motion

As shown in Fig.7, the extra variable r and s are introduced to identify the location of point D. When assuming α_1 and l_1 are known, the location of point A can be determined. Thus, we have

$$\begin{cases} r = \frac{3R}{2} - l_1 \cdot \cos \alpha_1 - c \cdot \cos \theta \\ s = l_1 \cdot \sin \alpha_1 - c \cdot \sin \theta \\ \alpha_4 = \arctan(s/r) \\ l_4 = \sqrt{s^2 + r^2} \\ T_4 = G \cdot \cos \alpha_1 / (\cos \alpha_4 \sin \alpha_1 + \sin \alpha_4 \cos \alpha_1) \\ T_1 = T_4 \cdot \cos \alpha_4 / \cos \alpha_1 \end{cases} \quad (6)$$

Discriminant relation is

$$|T_1 \sin \alpha_1 \cdot c \cdot \cos \theta + T_1 \cos \alpha_1 \cdot c \cdot \sin \theta - G(d \cos \theta + t \sin \theta)| < \varepsilon \quad (7)$$

Where ε is a small quantity.

Given the parameter $\alpha_1 \in (0^\circ, 90^\circ]$ (step is 0.01°), $l_1 = 300$ mm, $\theta \in (1^\circ, 30^\circ]$ (step is 2°). The simulation results are shown in Fig.8. And the relation between the changes of pitching angle θ and length l_2 in pitching motion, as shown in Fig. 9, shows the approximate linearity between θ and l_2 .

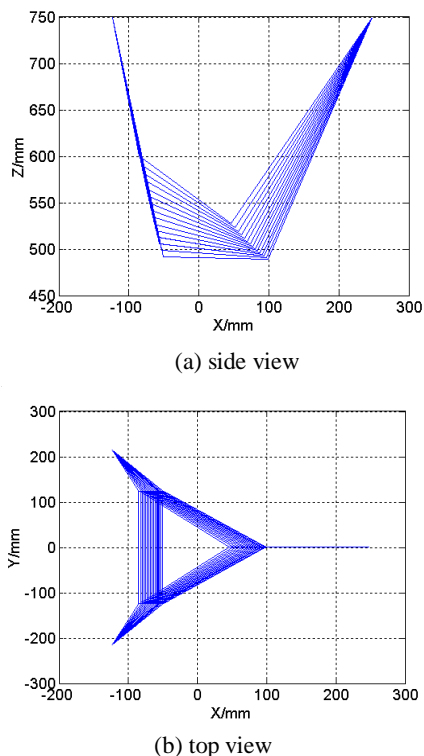


Fig. 8 The simulation of platform's pitching motion

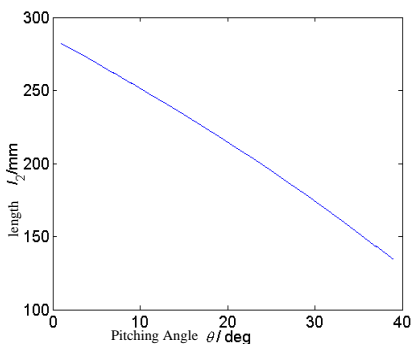


Fig. 9 Relation between the changes of pitching angle θ and l_2 in pitching motion

3.3 Heeling motion

The heeling motion is shown in Fig. 10. The corresponding kinematic equation can be expressed as equation set (8)

Where $\alpha_1, \alpha_2, \alpha_3, \beta_1, \beta_2, \beta_3, \gamma_1, \gamma_2, \gamma_3, T_1, T_2, T_3, l_1, l_2$ and l_3 are unknown variables, and heeling angle θ is known. For the convenience of solving, the functions related with $\alpha_1, \alpha_2, \alpha_3, \beta_1, \beta_2, \beta_3, \gamma_1, \gamma_2$ and γ_3 , and expressed as cosine function, such as $\cos\alpha_i, \cos\beta_i$ and $\cos\gamma_i$ ($i=1, 2, 3$), can be viewed as a variable.

Gauss-Newton method is used to solve the equations, and the simulation results are illustrated in Fig. 11.

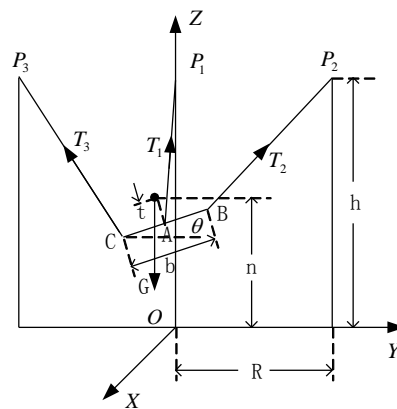
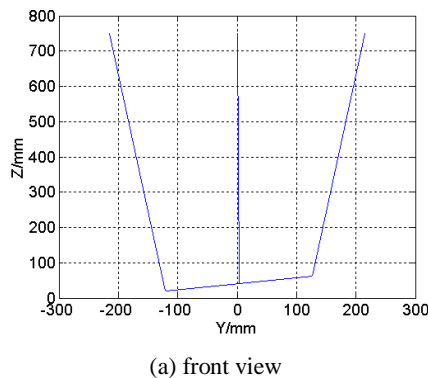


Fig. 10 Platform's heeling motion

$$\begin{cases}
 \cos^2 \alpha_1 + \cos^2 \beta_1 + \cos^2 \gamma_1 = 1 \\
 \cos^2 \alpha_2 + \cos^2 \beta_2 + \cos^2 \gamma_2 = 1 \\
 \cos^2 \alpha_3 + \cos^2 \beta_3 + \cos^2 \gamma_3 = 1 \\
 T_1 \cos \alpha_1 + T_2 \cos \alpha_2 = T_3 \cos \alpha_3 \\
 T_3 \cos \beta_3 + T_2 \cos \beta_2 = T_1 \cos \beta_1 \\
 T_1 \cos \gamma_1 + T_2 \cos \gamma_2 + T_3 \cos \gamma_3 = G \\
 -T_3 \cos \gamma_3 \cdot b \cdot \cos \theta - T_3 \cos \alpha_3 \cdot b \cdot \sin \theta \\
 -T_1 \cos \gamma_1 \cdot b \cdot \cos \theta / 2 + T_1 \cos \alpha_1 \cdot b \cdot \sin \theta / 2 \\
 + G(t \cdot \sin \theta + b \cdot \cos \theta / 2) = 0 \\
 -T_1 \cos \gamma_1 \cdot c - T_1 \cos \beta_1 \cdot b \cdot \sin \theta / 2 \\
 + T_3 \cos \beta_3 \cdot b \cdot \sin \theta + G \cdot d = 0 \\
 T_1 \cos \alpha_1 \cdot c - T_1 \cos \beta_1 \cdot b \cdot \cos \theta / 2 \\
 + T_3 \cos \beta_3 \cdot b \cdot \cos \theta = 0 \\
 l_2 \cdot \cos \alpha_2 + b \cdot \cos \theta + l_3 \cdot \cos \alpha_3 = \sqrt{3}R \\
 l_3 \cdot \cos \gamma_3 = l_2 \cdot \cos \gamma_2 + b \cdot \sin \theta \\
 l_3 \cdot \cos \beta_3 + c + l_1 \cdot \cos \beta_1 = 3R / 2 \\
 l_3 \cdot \cos \alpha_3 + b \cos \theta / 2 - l_1 \cdot \cos \alpha_1 = \sqrt{3}R / 2 \\
 l_3 \cdot \cos \gamma_3 = l_1 \cdot \cos \gamma_1 + b \cdot \sin \theta / 2
 \end{cases} \tag{8}$$



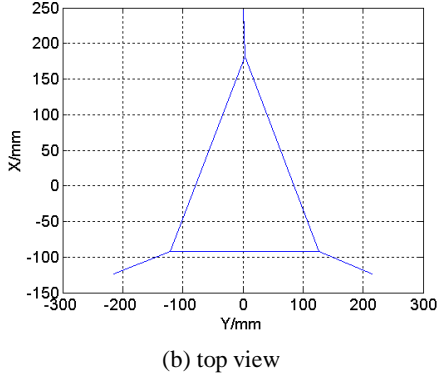


Fig. 11 The figure of platform's heeling motion ($\theta=10^\circ$)

From the heeling analysis, the center of platform drift 0.5mm~4.5mm from center of the base by $\Delta = l_1 \cdot \cos \beta_1$, when the heeling angle varies from 1° to 20° . Reduce the size of the platform or increase the height the pillar, the scope of heeling can be enlarged.

4. Static Analysis

On the base of kinematic analysis, the static analysis with three typical motion can be processed.

In horizontal up-down motion, according to the equation set (9), the tensions of T_1 and T_4 in wire of P₁A and P₄D can be expressed as

$$\begin{cases} \cos^2 \alpha_2 + \cos^2 \beta_2 + \cos^2 \gamma_2 = 1 \\ T_4 \cos \alpha_4 = 2T_2 \cos \alpha_2 \\ T_4 \sin \alpha_4 = 2T_2 \cos \gamma_2 \end{cases} \quad (9)$$

Where β_2 can be obtained by geometrical relationship as

$$\beta_2 = a \tan(l_4 / (3R / 2 - b / 2)) \quad (9)$$

Thus, for each specific pose of robot, the only set of tensions $[T_1 \ T_2 \ T_3]$, $T_i > 0 \ (i=1, 2, 3)$, $T_2 = T_3$, can be obtained.

Solving the equations (1), (9) and (10), get

$$\begin{cases} T_1 = Gd / (c \cdot \sin \alpha_1) \\ T_2 = T_3 = T_4 / 2\sqrt{1 - \cos^2 \beta_2} \end{cases} \quad (11)$$

Where, $\beta_2 = a \tan\left(l_4 / \left(\frac{3R}{2} - \frac{b}{2}\right)\right)$, $T_4 = \frac{G \cdot (c-d)}{\sin \alpha_4 \cdot c}$,

$$\alpha_1 = \tan^{-1} \frac{h-n}{\frac{c-d}{c} \left(\frac{3R}{2} - c\right)}, \quad \alpha_4 = \tan^{-1} \frac{h-n}{\frac{d}{c} \left(\frac{3R}{2} - c\right)}$$

As shown in Fig.12, the change of tension in the wire P₁A is small, but it is obvious in the wire P₂B and P₃C. For the case of pitching motion, according to the equation set (3) and (1), the tensions T_1 and $T_2(T_3)$ can be figured as Fig. 13. When pitching angle increases, the tension T_1 decreases and $T_2(T_3)$ increases. In the same way, the tensions in the case of heeling motion can be computed.

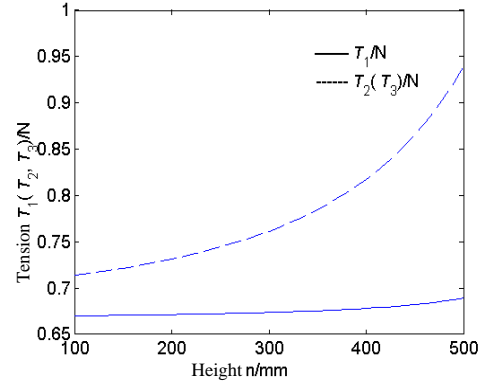


Fig.12 Tensions $T_1, T_2(T_3)$ in up-down motion

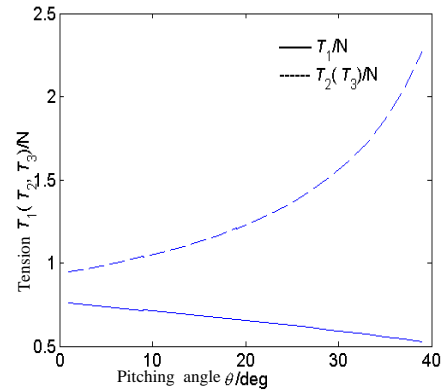


Fig. 13 Tensions $T_1, T_2(T_3)$ in pitching motion

5. Experiments of Prototype of the TWDP robot

The prototype of TWDP robot, as shown in Fig. 14, is manufactured as a principle demonstration. The control system of the robot is sketched as shown in Fig. 15. When the camera segment is included, the system is a close-loop control system, otherwise is an open-loop one.

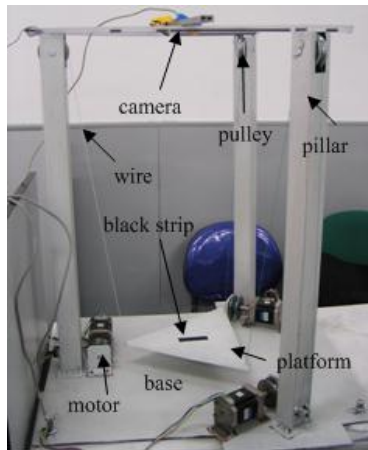


Fig.14The prototype the TWDP robo

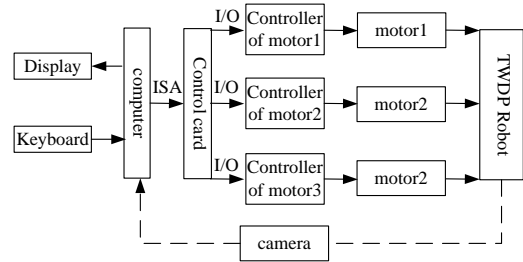


Fig.15 The cosntrl system structure of robot

5.1 Open-loop Control

By the relatively high precision of stepper motor, the open-loop control scheme can be used.

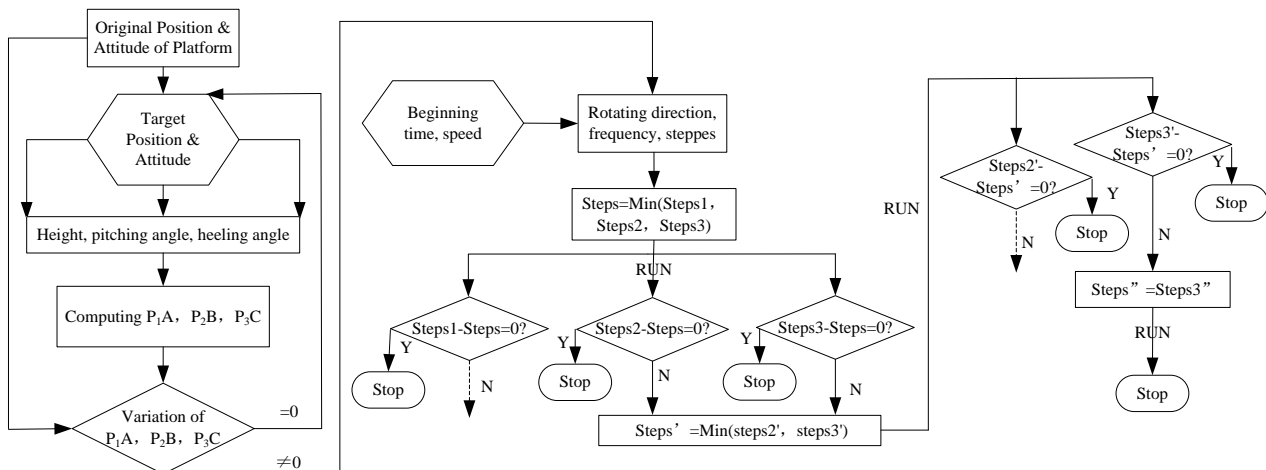


Fig.16 Open loop control figure of robot system

In open-loop control scheme, as shown in Fig. 16, according to the requirement of target position and attitude of the platform, the running time and speed, the running frequencies and steppes of three stepper motor can be calculated separately. Because the motors equipped in the prototype can only be run under the same frequency, when different running steppes are needed, the three motors run the same steppes first,

and then motors taking more steppes continue to run. Which can be called motion decomposing.

5.2 Close-loop Control

Adding feedback segment into the open-loop control scheme, a simple close-loop control system can be set up as illustrated in Fig. 15.

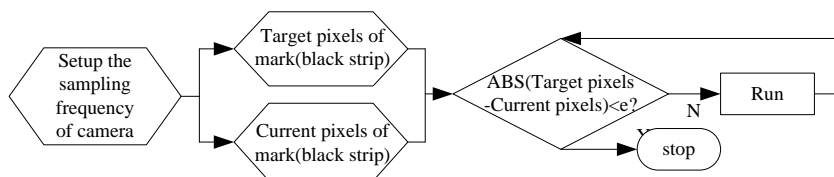


Fig. 17 Close-loop control of robot system

In the feedback segment, the image processing technique based machine vision is used to monitor the position and attitude of target (platform) real-timely. When the platform moves to the specified position, the motors are controlled to stop by feedback of camera, that is, the camera is fixed on the top of the robot and the platform is controlled to run or stop by the comparison of target pixels of mark(black strip) and current pixels of mark, as shown in Fig. 17.

Step 1: Stick a black or fuscous mark as identifying target, which is used to be monitoring. The black or fuscous is chosen to distinguish the background of robot.

Step 2: Make “Height-Pixels” query table according to specified height of the platform. When the platform is designated to a specified position, the corresponding pixels of mark can be read from it. When the value of height is not in the table, the following interpolation formula can be used as approximation

$$\text{Target Pixels} = \frac{\text{Pixels A}-\text{Pixels B}}{2} \quad (12)$$

Where Pixels A and Pixels B are the value of pixel located nearest the designated height in the “Height-pixels” table. (Height B < Designated Height < Height A)

Step 3: When the pixels corresponding to the designated height is obtained, the current pixels of mark is compared with it, and the running direct of motor then can be decided.

Step 4: Repeat Step 3, and stop the motors until the difference of the current pixels and target pixels is smaller than a pre-initialized value.

The once image processing is shown in Fig. 18.

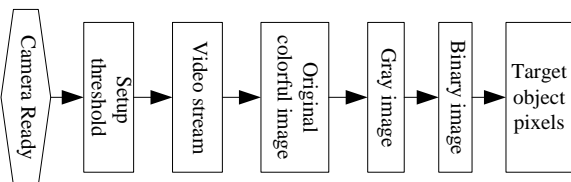


Fig. 18 Once image processing flow chart

6. Experiment and Error Analysis

According to the open-loop and close-loop control scheme, the control programs are developed. The main interface of

program is shown in Fig. 19.



Fig.19 Main form of control program

When the open-loop experiment is carried out, choose the motors that need to run and corresponding running direction, and input the running frequency and running steps, the robot can move then.

When the close-loop experiment is carried out, input the expected height of platform and click “Image-processing” button, can camera can be modulated to get better original image, gray image and binary image, as shown from Fig. 20(a) to Fig. 20(c)



(a) original image



(b) gray image



(c) binary image

Fig. 20 Images in the close loop control

From the experiment, the robot can be controlled well either with open-loop mode or with close-loop mode. However, the movement precision are restricted by un-avoided errors. From error analysis, the following factors can be ascribed:

(1) Inherent Errors. Instead of traditional hydraulic cylinder or lead screw, the wires, whose elasticity are affected much by the change of load and motion, are used as driving component, which can be presented markedly in high speed and big load case and will result in relatively large motion error.

(2) Errors from manufacturing and assembling. These errors come from the manufacturing errors of driving pulley shaft connected with the motor shaft, the assembling error of driven pulley, and the variation of wire winding position on the pulleys. Which are main errors affecting the robot studied in this paper.

(3) Errors of stepper motor. The stepper motors used in the robot here there does exist errors in precisely locating of platform. Considering the only principle experiments in the paper, the errors of stepper motor can be neglected.

Thus, the following methods can be adopted to reduce the errors from the above error analysis.

(1) Wires with big Young's Modulus are suggested in the design of such wire-driven robot.

(2) Improve manufacturing and assembling precision.

(3) Real-time kinematic computation to compensate the driving wire length error.

7. Conclusion

In the paper, a novel new gravity-constrained (GC) three-wire-driven (TWD) parallel robot is proposed and the prototype of it is manufactured and assembled.

(1) With its mechanism model, three typical kinematic analytical models, including horizontal up-down motion, pitching motion and heeling motion, and their corresponding simulations are given in detail. The simulation results show the robot has good movement stability. The paper can provide useful materials to study of dynamics and control on wire-driven robot.

(2) The open-loop and close-loop control scheme are used separately to realize the motion control of the robot. Especially, the image processing based machine vision is adopted firstly in the close-loop control of wire-driven robot. At last, the error analysis of the robot is given in detail. And the methods of improving the moving precision are listed.

The robot proposed here is proved having good controllability. With the structure of gravity-constrained (GC) three-wire-driven (TWD) parallel robot can be used as trainer to simulate the moving of ship and also as transiting equipment in heavy load situation.

References:

- [1] N. G. Dagalakis, J. S. Albus, B.-L. Wang, J. Unger, and J. D. Lee. Stiffness study of a parallel link robot crane for shipbuilding applications[J]. *Journal of Offshore Mechanics and Arctic Engineering*, Vol.111, No.3, 1989, pp. 183-193.
- [2] S. Tadokoro, S. Nishioka, T. Takamori, and K. Maeda. On fundamental design of wire Configurations of wire driven parallel manipulators with redundancy[C]. *Proceedings of Japan-U.S.A. Symposium on Flexible Automation*, Vol.1, 1996, pp.151-158.
- [3] P.G. Clem, M. Rodriguez, J.A. Voigt and C.S. Ashley, U.S. Patent 6,231,666. (2001)
- [4] Sadao Kawamura, Hitoshi Kino and Choe Won, High-speed manipulation by using parallel wire-driven robots[J], *Robotica*, Vol.18, No.1, 2000, pp.13-21.

[5] J. Albus, R. Bostelman, and N. Dagalakis. The nist robocrane[J]. *J. of Robotic Systems*, Vol.10, No.5, 1993, pp.709-724.

[6] T. Maier, C. Woernle. Kinematic Control of Cable Suspension Robots. *Proceedings of the NATO-ASI Computational Methods in Mechanisms*, Vol. 2, 1997, pp. 421-430.